Semi-Automatic Extraction of The Threshold Segmentation of Coastline Based on Coastline Type

To cite this article: Tan Yu *et al* 2021 *IOP Conf. Ser.: Earth Environ. Sci.* **690** 012019

Semi-Automatic Extraction of The Threshold Segmentation of Coastline Based on Coastline Type

Tan Yu*, Shuwen Xu, Xinyu Zhou, Jiajun Xiao, and Bingxu Zhang

College of Marine Sciences, Shanghai Ocean University, Shanghai 201306, China

*E-mail: tyu@shou.edu.cn

Abstract. Using remote sensing images to extract the shoreline is an important means of studying coastlines. In this paper, we propose a semi-automatic coastline extraction method based on the coastline type that uses region segmentation and edge detection image processing. Based on selected Landsat 4-5 TM and Landsat 8 OLI_TIRS satellite images of Chongming Island from 1985 to 2017, we find that the point control method, neighborhood marking method, and targeted selection based on different shoreline types significantly improve the calculation efficiency, have good adaptability, and produce highly accurate shoreline extraction.

1. Introduction

Changes in the coastline and the accumulation trends of coastline erosion provide important information for coastal management, as they can help determine the long-term shoreline erosion rates and predict future shoreline locations [1,2]. The methods used to extract the coastline from satellite images mainly comprise automatic extraction, semi-automatic extraction, and visual interpretation. Erteza [3] proposed an automated method that comprises three main shoreline extraction algorithms: an image preprocessing step that emphasizes the land-and-sea boundary, the generation of a coastline from the coastal land boundaries, and the identification and marking of islands. Wang et al. [4] proposed a new method of automatically extracting coastlines from high-resolution IKONOS images. First, a mean shifting segmentation algorithm is used to segment the image into uniform regions to extract the preliminary shoreline, and a local threshold segmentation method is then used to locally refine the shoreline. Using a pixel-based classification method, Sabuncu et al. [5] analyzed the land cover types of the study area and conducted a geodetic survey to detect the coastline deformation. Vasilis et al. [6] proposed a coastline estimation algorithm that automatically extracts coastlines using edge detection and optimization. Dellepiane et al. [7] developed an algorithm based on fuzzy connectivity and interferometric synthetic aperture radar measurements to semi-automatically extract coastlines. Shu et al. [8] semi-automatically extracted the Pacific coastline of Canada from RADARSAT-2 images by narrow-band level set segmentation. Billa et al. [9] proposed a semi-automatic technique that uses enhanced filtering techniques to identify and extract coastlines from RADARSAT-1 satellite imagery. Based on the coverage information of WorldView-2 satellite imagery, Wassie et al. [10] explored the potential of mean shift segmentation in QGIS and semi-automatically extracted terrestrial boundaries.

The advantage of the automated and semi-automated extraction of shorelines is that these methods offer high precision, fast speed, independent referencing, good adaptability, and stability. Moreover, the manual shoreline measurement methods are difficult and expensive to implement. In particular, the

non-automatic coastal detection methods require visual interpretation of high-resolution aerial photographs and are thus time-consuming and require complex processing skills. Therefore, it is necessary to examine the methods for extracting the coastlines from remote sensing images of coastal areas [11].

There are numerous methods for conducting automatic coastline extraction, including the active contour model method, region growth extraction, mathematical morphology method, neural network classification, threshold segmentation (also known as density segmentation), and edge detection. Edge detection is used to detect the points with the most obvious gray level changes in the images. To determine whether the gray level change of an edge point is severe or not, the gradient threshold is set as the evaluation standard. Thus, selecting the threshold is an important component of edge detection, with the main methods of threshold selection being the global threshold method and the local threshold method.

The global threshold method uses a single threshold for the whole image, compares the gray value of each pixel in the image with the threshold, and then transforms the gray images into binarization images. The global threshold method is mainly divided into two classical methods: Otsu's thresholding method [12] and the maximum entropy method [13] .

The principle of Otsu's thresholding method is to select a specific threshold to divide the pixels into two classes: target and background. The greater the inter-class variance between the two classes, the greater the difference between them. Otsu's method has been widely used because it is simple and effective [14]. However, with the increasing numbers of image types, Otsu's method takes too much time to select a multi-level threshold [15] and is thus not very efficient.

The maximum entropy threshold selection method [13], which was proposed by Kapur et al. in 1985, is based on the definition of the information entropy, with the threshold T being solved to maximize the sum of the information entropy of the target and the background, or in other words, to determine the best uniformity of the target and the background. In 1989, Abutaleb et al. [16] extended the one-dimensional maximum entropy method proposed by Kapur et al. [13] to a two-dimensional approach that also considers the pixel gray information and its neighborhood spatial information and that has strong anti-interference ability.

The local threshold method involves calculating one or more threshold values based on certain attributes of a central pixel and its neighborhood, and the discriminant of the threshold value. The main local threshold methods are the Niblack algorithm [17] and Bernsen algorithm [18] .

The Niblack algorithm takes the mean and standard deviation of the point in the $\mathrm{r} \times \mathrm{r}$ neighborhood with (i,j) as the center, and the threshold of the center point is calculated as [17]:

$$\mathrm{T(i,j)} = \mathrm{m}(i,j) + k * s(i,j) \tag{1}$$

where $\mathrm{T(i,j)}$ is the threshold , $\mathrm{m}(i,j)$ is the sample average, $s(i,j)$ is the standard deviation, and k is the correction coefficient.

Although the Niblack algorithm produces better results than the other local threshold methods, it has limitations in terms of the selection of the neighborhood size. In particular, the neighborhood must be small enough to preserve the local details and large enough to suppress the noise, so the choice of neighborhood is complex [19].

The Bernsen algorithm takes the maximum pixel Z_h and the minimum pixel Z_l in the $\mathrm{r} \times \mathrm{r}$ neighborhood centered on (i,j), and the threshold of the center point is calculated as [18]:

$$\mathrm{T}(i,j) = (Z_h + Z_l)/2 \qquad (Z_h - Z_l) \le l \tag{2}$$

where l is the contrast threshold. Although the algorithm can adaptively select the threshold according to the local gray characteristics and has strong flexibility, its performance is hindered by the ghost shadows and broken lines generated in the binarization process [20] .

In recent years, the methods of extracting the coastline based on the coastline type have received increasing attention. Zhang et al. [21] summarized the distribution of various types of coast in Fujian Province and their interpretation signs. Then, based on the coastline formula, they modified the shoreline in ArcGIS and completed the extraction of the coastline. This resulted in a clearer image of

the land and maritime border, and improved the accuracy of the water sideline extraction. Jianzhong et al. [22] used two methods to extract two different types of coastline, and achieved satisfactory results. They proved that extracting the coastline based on the coastline type is a feasible and effective approach. However, while their approach is more accurate and targeted, it mostly involves visual interpretation, is only suitable for single research areas, and the extraction methods are complex and have poor universality.

To accurately select the coastline, improve the accuracy and speed of the coastline extraction, and improve the discontinuity of the traditional local threshold in the process of binarization, we propose a threshold segmentation method based on the coastline type.

2. Data source and Research Area

The research area examined in this paper is Chongming Island (121.13°E-122.03°E, 31.11°N-31.76°N, Figure 1), located in the Yangtze River Estuary. In addition to being the third largest island in China and the largest alluvial island in the world, Chongming Island is an important strategic area for the sustainable development of Shanghai, with the ongoing erosion of its coastline being inextricably linked to the local ecology. The Yangtze River carries large amounts of sediment to the estuary, which make the tidal resources along the coast of Chongming Island very rich, especially in the Dongtan area. These resources support the expansion of the coastal wetlands and the swamp vegetation [23]. On the mudflat frontier, positive interactions between the vegetation establishment and sedimentation processes may lead to the expansion of the mudflats and increased vegetation. The growth of the tidal flats along the Yangtze River estuary and the increased swamp vegetation are caused by the strong stimulation from the short-term river sand flow [24].

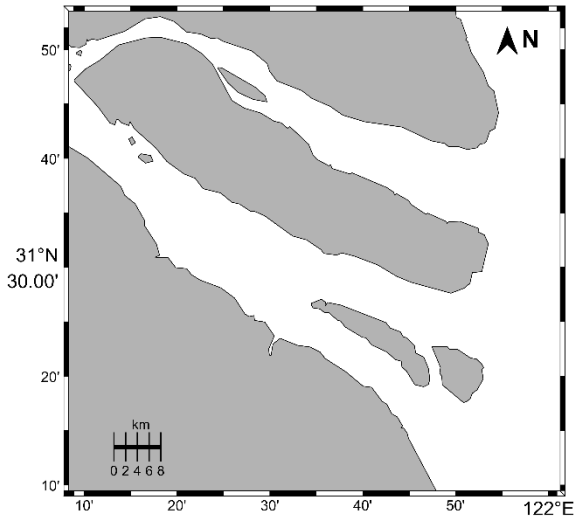

Figure 1. The research area is Chongming Island (121.13°E-122.03°E, 31.11°N-31.76°N), located in the Yangtze River Estuary.

The remote sensing data used in this paper were sourced from the Landsat series of satellite images. Specifically, we use the Landsat5-TM images for 1985, 1990, 1995, 2000, and 2005, and the Landsat8-OLI images for 2009, 2013, and 2017. The data set was provided by the Geospatial Data Cloud site hosted by the Computer Network Information Center of the Chinese Academy of Sciences (http://www.gscloud.cn).

All of the selected images were subjected to system radiation correction and geometric correction. The basic information of each data source is shown in Table 1 below.

Table 1. Basic information about the data source.

Year	Sensor type	Acquisition time	Band	Time resolution /day	Spatial resolution /m
1985	Landsat5-TM	1985-11-20	Mid-infrared	16	30
1990	Landsat5-TM	1990-12-04	Mid-infrared	16	30
1995	Lansdat5-TM	1995-05-08	Mid-infrared	16	30
2000	Landsat5-TM	2000-05-21	Mid-infrared	16	30
2005	Landsat5-TM	2005-06-04	Mid-infrared	16	30
2009	Landsat5-TM	2009-07-17	Mid-infrared	16	30
2013	Landsat8-OLI	2013-08-29	near-infrared	16	30
2017	Landsat8-OLI	2017-07-23	near-infrared	16	30

Due to the wide coverage of the satellite imagery, when we conduct point control on the original images, we ignore the details and inaccurately extract the shoreline. Therefore, as shown in Figure 2 we select the research area for Chongming Island area based on the UTM coordinates of the image (323122-418787, 3443118-3530734), which is convenient for follow-up work.

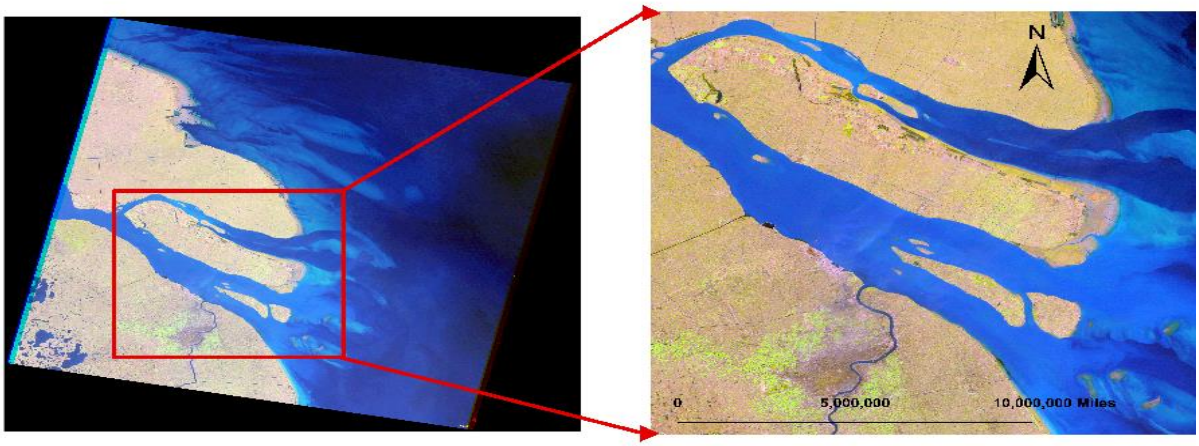

Figure 2. In order to extract the shoreline more accurately, the scope of the study is enlarged and framed.

3. Methods

In this study, we improve the traditional local threshold method by using region segmentation and edge detection image processing based on the coastline type to generate more accurate and adaptive extraction results.

3.1. Filter Method Selection

Although satellite remote sensing images have good spatial coverage, they tend to be affected by noise and deformed by light and cloud. Therefore, the images require filtering to improve the image deformation. As shown in Figure 3, we use Gaussian filtering, mean filtering, and median filtering to reduce the noise and enhance the edges. We find that Gaussian filtering is the most efficient method because it eliminates the noise while keeping the image smooth. In contrast, although the median filter and averaging filter eliminate the noise, they blur the edges of the images, especially in the coastline area. Thus, the images are not very clear, and the accuracy is reduced when extracting the shoreline.

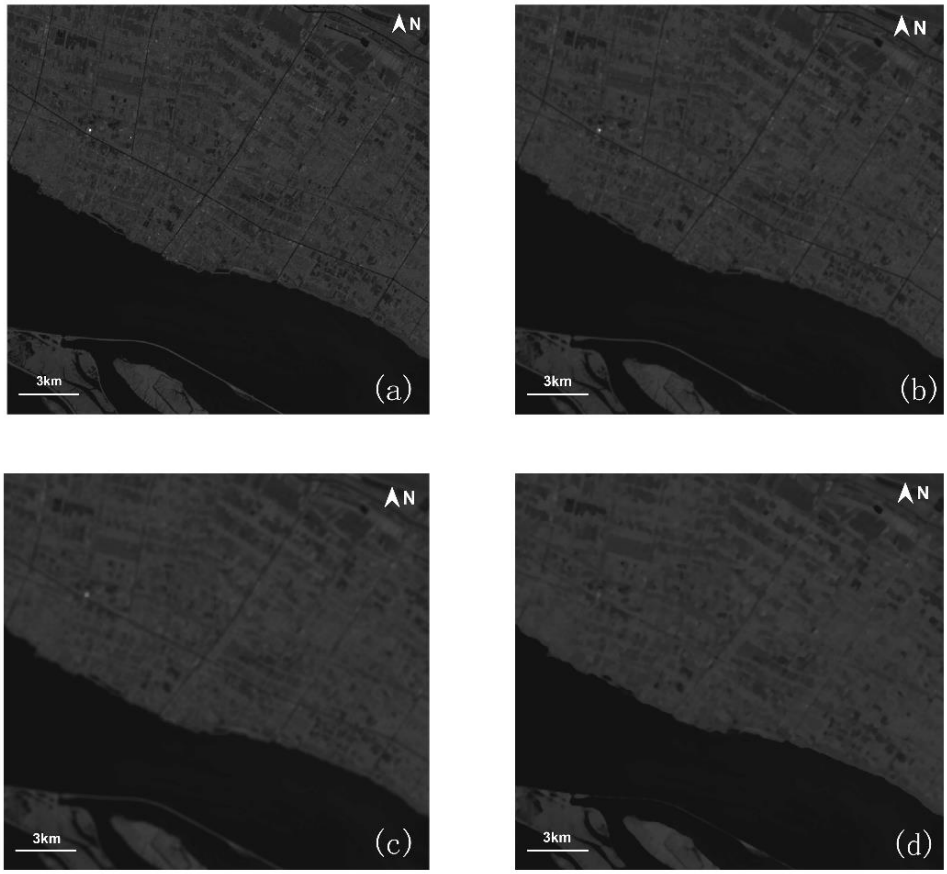

Figure 3. The picture shows the comparison of the effect of the three filters((a) Original image (b)Gaussian filtering (c)Mean filtering (d)Median filtering) on the original image. It can be seen that the Gaussian filter is better.

3.2. Local Threshold Method Based on Shoreline Type: the Point Control Method

Because the global threshold method is applicable to remote sensing images with small gray scale gradients on the sea and land borders, especially for images with uneven gray distribution, the images cannot be correctly segmented by land and sea. Moreover, the selection of a single threshold can only reflect the edge information of a single shoreline, and the details of the shoreline extraction are not accurate. The traditional local threshold method divides the original image into smaller images, adaptively adjusts the threshold according to the characteristics of the local area pixel gray distribution,

and then selects the corresponding threshold for each sub-image. However, this approach is not very efficient.

The remote sensing images are large, and factors such as the brightness, contrast, resolution, and noise are unevenly distributed. Before performing the image binarization, based on the image segmentation idea of the local threshold method, we divide the image into 15 blocks. According to the different shoreline types, we apply the point control method using the cross cursor to precisely select the sea-land boundary points to return the coordinate values.

Table 2. Pixel normalized values.

year	sandy shoreline	artificial shoreline	silt shoreline	data source
1985	0.1466	0.1149	0.0532	
1990	0.1464	0.1052	0.046	
1995	0.1520	0.0890	0.0480	Landsat5-T
2000	0.1542	0.1219	0.0671	M
2005	0.1046	0.1145	0.0854	
2009	0.232	0.2226	0.1315	
2013	0.1371	0.1364	0.1206	Landsat8-O
2017	0.1194	0.1299	0.1095	LI

As shown in Table 2, for the Landsat5-TM satellite images, the normalized average of the sandy shoreline pixels ranges from 0.1046 to 0.2320, with an average of 0.1560 over the sample period. The average range of the artificial mean line pixel normalization is 0.0890-0.2226, with an average of 0.1280 over the sample period. The normalized average of the muddy shoreline pixels ranges from 0.0460 to 0.1315, with a multi-year average of 0.0719.

For the Landsat8-OLI satellite images, the normalized average of the sandy shoreline pixels ranges from 0.1194 to 0.1371, with a multi-year average of 0.1283. The average range of the artificial mean line pixel normalization is 0.1299-0.1364, and the average over the sample period is 0.1332. The average normalized pixel of the muddy shoreline ranges from 0.1095 to 0.1206, with an average of 0.1151.

In most cases, the pixel normalized mean is sandy shoreline > artificial shoreline > silt shoreline. Moreover, the normalized averages of the pixels of the sandy shoreline and the artificial shoreline are relatively close, probably due to the proximity of the reinforced concrete material and the sandy material.

3.3. Select Threshold Scaling Range

The shoreline of Chongming Island mainly comprises artificial, sandy, and silt shorelines. We calculate the average pixel values in the neighborhood range. We then select the maximum difference between a value and the average value in the neighborhood, and we use the minimum value as the threshold scaling range value.

The east beach of Chongming Island comprises a silt shoreline with significant sediment accumulation, and the pixel gray levels are thus lower in the remote sensing images. Therefore, the threshold scaling range of the sub-image based on the muddy shoreline is used to select the minimum value of the difference. The rest of Chongming Island is dominated by sandy and artificial shorelines, which have high grayscale pixel values in the remote sensing images due to the clear edge of the shoreline. Therefore, the partial sub-image threshold scaling range is used to select the maximum value of the difference in the neighborhood.

3.4. Shoreline Extraction: Neighborhood Marking Method

After selecting the appropriate threshold, the images are binarized and the approximate values of the brightness gradients are calculated using the edge detection algorithm. The edge points with sudden variations of grayscale gradient are then detected to solve the problem of coastline discontinuity and extract the point set of the coastline.

Our specific approach is to use the sea and land boundary points selected by the first sub-image as the starting point (the sea-land boundary points can be selected according to the type of coastline to be extracted). The neighborhood is then selected with this point as the center point, and the point within the neighborhood is judged to be 1 (after binarization, the land is 1, the ocean is 0, and the extracted point set is 1). If the nearest point in the neighborhood is more than one, we select the corresponding point according to the trend of the coastline to the mark and then use this point as the next center point to select the subsequent neighborhood.

4. Result

This study uses Landsat 4-5 TM and Landsat 8 OLI_TIRS images from 1985, 1990, 1995, 2000, 2005, 2009, 2013, and 2017. Based on the idea of local threshold segmentation, each image is divided into multiple regions. We select the threshold and its range for the different coastline types and extract the coastline of Chongming Island (Figure 4 and Figure 5). Comparison of the extracted coastline and the remote sensing image shows that the accuracy of the result is good. The degree of erosion in the area can then be observed from the changes in the coastline from 1985 to 2017.

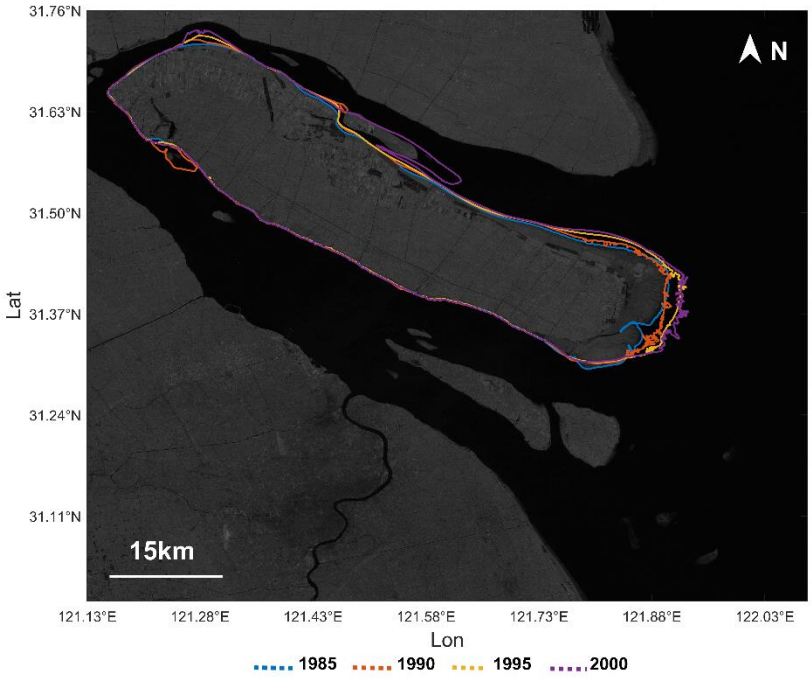

Figure 4. Shoreline extraction results for 1985-2000 show that the shoreline changes of Chongming Island are concentrated in Dongtan and North Branch.

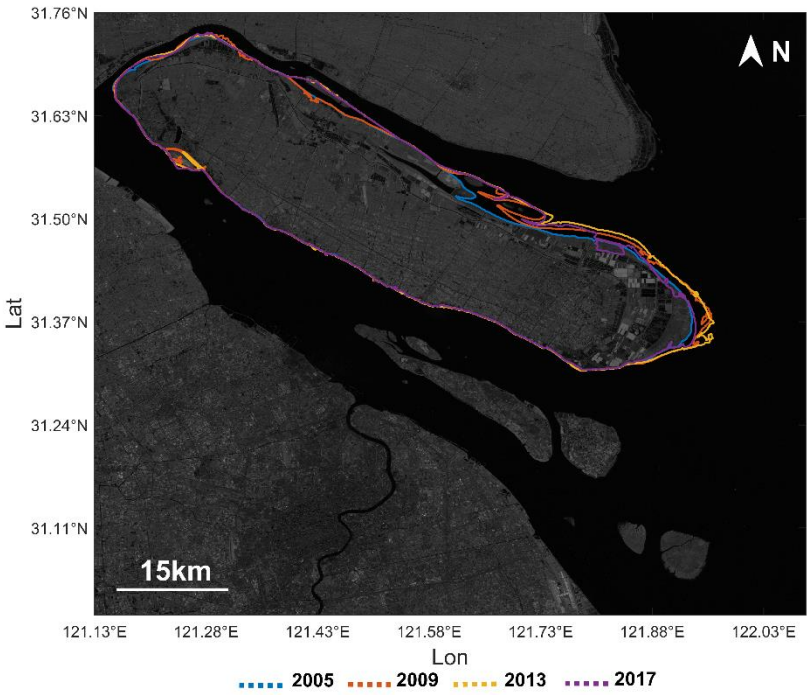

Figure 5. Shoreline extraction results for 2005-2017 show that the Dongtan area continues to expand eastwards, forming a cone, and the north branch gradually connects with the north of Dongtan.

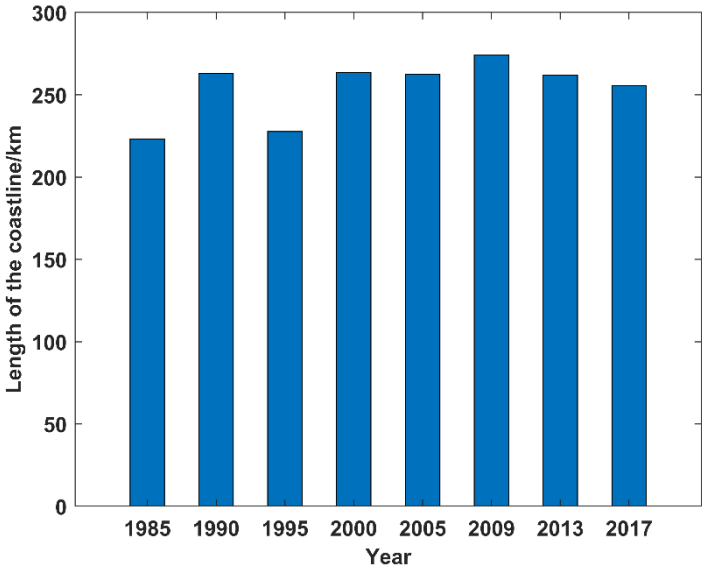

Figure 6. The length of the Chongming Island shoreline from 1985 to 2017 changes gradually slowed down, depending on the changes in Dongtan area.

According to the Figure 6, from 1985 to 1990, the length of the coastline of Chongming Island showed an increasing trend, with an overall increase of 39.71 km. From 1990 to 1995, the coastline length showed a decreasing trend, with an overall decrease of about 53.16 km. From 1995 to 2000, the coastline length again showed an increasing trend, with an overall increase of about 35.91 km. From 2000 to 2005, the overall coastline length showed a slight decreasing trend, with a decrease of about

1.14 km. From 2009 to 2013, the coastline length showed a decreasing trend, with a decrease of about 12.36 km. From 2013 to 2017, the coastline also showed a decreasing trend, with the overall length being reduced by about 6.21 km.

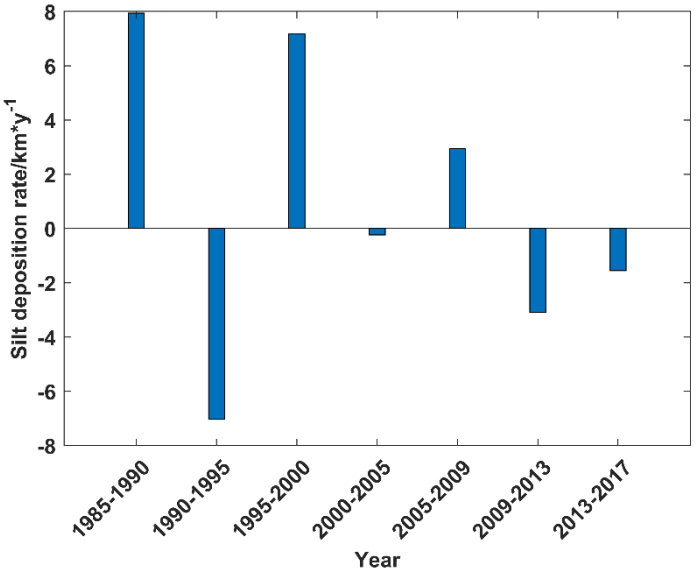

Figure 7. The rate of siltation on the coastline of Chongming Island is declining, or it may be related to the Three Gorges Dam.

According to the Figure 7, from 1985 to 2017, the average siltation rate of Chongming Island was 0.88km/y. From 1985 to 1990, the silt accumulated at a rate of 7.94 km/y. From 1990 to 1995, it eroded at a rate of 7.03 km/y. From 1995 to 2000, it accumulated at a rate of 7.18 km/y. From 2000 to 2005, it eroded at a rate of 0.23 km/y. From 2005 to 2009, it accumulated at a rate of 2.94 km/y. From 2009 to 2013, it eroded at a rate of 3.09 km/y. From 2000 to 2005, it eroded at a rate of 1.55 km/y.

Overall, the length of the coastline of Chongming Island changed most obviously between 1985 and 2000. After 2000, the variation in the length of the coastline clearly slowed down. The shoreline siltation mainly occurred on the northern branch of Chongming Island and in the Dongtan area. After several decades of changes, the northern branch islands have continued to expand and have connected to the mainland of Chongming Island, and the Dongtan area has extended to the East China Sea to form tidal wetlands.

Due to the cofferdam, the body sand on the northern branch of Chongming Island accumulated rapidly over the sample period, and the accumulated sand expanded to connect Chongming Island with the mainland.

In the early part of the sample period, the high-strength cofferdams on Chongming Island promoted siltation and had a positive impact on the development of the Dongtan area by accelerating the siltation in the East China Sea. However, the construction of the Three Gorges Dam and the planting of the shelter forests have reduced the amount of sediment in the Yangtze River and hindered the development of the tidal flats in the Dongtan area.

5. Discussion

Our semi-automatic method for extracting the local threshold coastline based on the coastline type is very efficient. In the process of extracting multiple images of the coastline, it takes about seven seconds on average to manually select the sea and land boundary points of the different coastline types in each region, and the overall coastline extraction takes about five seconds on average. During the coastline extraction process, the length of the coastline can also be calculated.

Shu [8] used a semi-automatic method of extracting coastlines from RADARSAT-2 intensity images, and found that when the threshold intensity was 98, the calculation took 10.5 seconds, and when the threshold intensity was 50, the calculation took 26.3 seconds. Using cellular automata, Feng [25] extracted the Dongtan area of Chongming Island in 15 seconds. Thus, our results show that the proposed method is effective and feasible for coastline extraction.

Finally, to evaluate the accuracy of our method, we artificially selected 30 sea-land boundary points on the satellite images and recorded their positions using the ENVI software platform(Figure 8). We then compared the results with the extracted coastline, and the position error was about 1.16 pixels. These results show that our semi-automatic method of extracting the local threshold coastline based on the coastline type is highly accurate and can be applied to shoreline extraction in most sea areas.

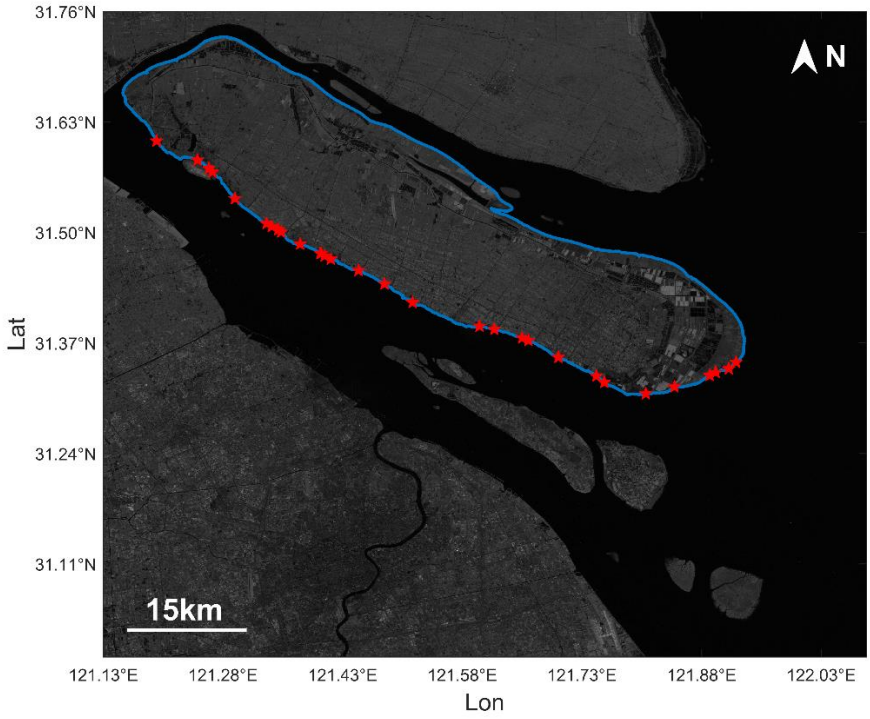

Figure 8. Accuracy reference point (the red points are the 30 reference points selected in ENVI and the blue line is the shoreline extracted by this method).

6. Concusion

Using region segmentation and edge detection image processing methods, we propose a semi-automatic coastline extraction method based on the coastline type. The use of the point control and neighborhood marking methods significantly improves the calculation efficiency of the algorithm, which has good adaptability and provides highly accurate coastline extraction.

It is found that the coastline changes mainly occur in the northern branch and Dongtan area of Chongming Island, with the coastline expanding to the East China Sea. The coastline undergoes significant changes before 2000 and then remains relatively stable after 2000.

We have also developed our approach as software, which can be used to extract coastlines from select images (Figure 9).

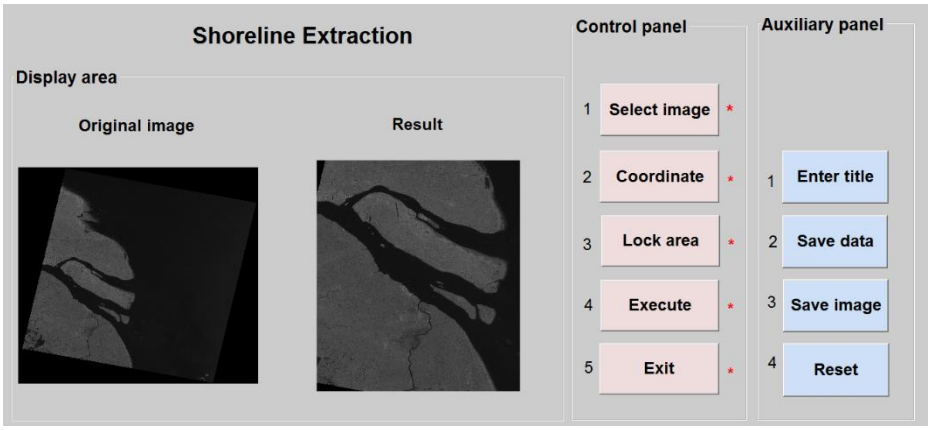

Figure 9. Welcome to the developed software interface. The operation of the software is very simple and efficient.

Because the quality of image is an important influencing factor in coastline extraction, the differences between the pixel values in images of sea and land and whether the boundary between the sea and land is clear are key factors affecting this method. Therefore, in future work, we intend to further improve the accuracy of coastline estimation by adding image edge smoothing to the image segmentation to make the coastline extraction more accurate.

Acknowledgements
The authors thank Geospatial Data Cloud site, hosted by the Computer Network Information Center of, the Chinese Academy of Sciences for the Landsat 4-5 TM and Landsat 8 OLI_TIRS satellite data. The authors also thank The National Natural Science Foundation [grant number 41906152]. The Open Fund of the Key Laboratory of Ocean Circulation and Waves, the Chinese Academy of Sciences [KLOCW1801]; National Key Research and Development Program of China [grant number 2018YFC0213103]; National Natural Science Foundation [grant number 41606196]; Shanghai Student Innovation Program S201810264019; and 2019 Shanghai Municipal Education Commission undergraduate key courses A1-2005-00-200105.

References
[1] Boak, E H and I L Turner. 2005 Shoreline definition and detection: a review. *Journal of Coastal Research* **21** 688-703.
[2] Douglas, B C and M Crowell. 2012 Long-term shoreline position prediction and error propagation. *Journal of Coastal Research* **16** 145-152.
[3] Erteza, I A. 1998 An automatic coastline detector for use with SAR images. United States: Sandia National Laboratories (SNL-NM), Albuquerque, NM.
[4] Frazier, P S and K J Page. 2000 Water body detection and delineation with Landsat TM data. *Photogrammetric engineering and remote sensing* **66** 1461-1468.
[5] Sabuncu, A, A Dogru, H Ozener and B Turgut. 2016 Detection of coastline deformation using remote sensing and geodetic surveys. *International Archives of the Photogrammetry, Remote Sensing and Spatial Information Sciences* **8** 1169-1174.
[6] Paravolidakis, V, L Ragia, K Moirogiorgou and M Zervakis. 2018 Automatic coastline extraction using edge detection and optimization procedures. *Geosciences* **8** 407-425.
[7] Dellepiane, S, D R Laurentiis and F Giordano. 2004 Coastline extraction from SAR images and a method for the evaluation of the coastline precision. *Pattern Recognition Letters* **25** 1461-1470.
[8] Shu, Y M, J Li and G Gomes. 2010 Shoreline extraction from RADARSAT-2 intensity imagery using a narrow band level set segmentation approach. *Marine Geodesy* **33** 187-203.
[9] Billa, L and B Pradhan. 2011 Semi-automated procedures for shoreline extraction using single

RADARSAT-1 SAR image. *Estuarine, Coastal and Shelf Science* **95** 395-400.
[10] Wassie, Y A, M N Koeva, R M Bennett and C H J Lemmen. 2018 A procedure for semi-automated cadastral boundary feature extraction from high-resolution satellite imagery. *Journal of Spatial Science* **63** 75-92.
[11] Mirsane, H, Y Maghsoudi, R Emadi and M Mostafavi. 2018 Automatic Coastline Extraction Using Radar and Optical Satellite Imagery and Wavelet-IHS Fusion Method. *International Journal of Coastal and Offshore Engineering* **2** 11-20.
[12] Otsu, N. 2007 A Threshold Selection Method from Gray-Level Histograms. *IEEE Transactions on Systems Man & Cybernetics* **9** 62-66.
[13] Kapur, J N, P K Sahoo and A K Wong. 1985 A new method for gray-level picture thresholding using the entropy of the histogram. *Computer vision, graphics, and image processing* **29** 273-285.
[14] Qu, Z and L Zhang. 2010 Research on Image Segmentation Based on the Improved Otsu Algorithm. In *International Conference on Intelligent Human-machine Systems & Cybernetics*, 228-231.
[15] Sahoo, P K, S Soltani and A K Wong. 1988 A survey of thresholding techniques. *Computer Vision Graphics & Image Processing* **41** 233-260.
[16] Abutableb, A S. 1989 Automatic thresholding of gray-level pictures using two-dimensional entropy. *Computer Vision Graphics & Image Processing* **47** 22-32.
[17] Niblack, W. 1985 *An introduction to digital image processing*. Strandberg Publishing Company.
[18] Bernsen, J. 1986 Dynamic thresholding of gray-level images. *Proceedings of the Eighth International Conference Pattern Recognition* 1251-1255.
[19] Khashman, A and B Sekeroglu. 2007 A novel thresholding method for text separation and document enhancement. In *Proceedings of the 11th panhellenic conference on informatics*, pp.324-330.
[20] Pan, M, F Zhang and H F Ling. 2007 An image binarization method based on HVS. In *IEEE International Conference on Multimedia and Expo*, 1283-1286: IEEE.
[21] Zhang, H N, Q G Jiang and X Jiang. 2013 Coastline Extraction Using Support Vector Machine from Remote Sensing Image. *Journal of multimedia* **8** 175-182.
[22] Yin, J Z and F Q He. 2011 Researching the Method of Coastline Extracted by Remote Sensing Image. *Remote Sensing, Environment and Transportation Engineering* 3441-3444.
[23] Ge, Z M, H B Cao, L F Cui, B Zhao and L Q Zhang. Future vegetation patterns and primary production in the coastal wetlands of East China under sea level rise, sediment reduction, and saltwater intrusion. *Journal of Geophysical Research Biogeosciences* **120** 1923-1940.
[24] Hu, M Y, Z M Ge, Y L Li, S H Li, L S Tan, L N Xie, Z J Hu, T Y Zhang and X Z Li. 2019 Do short-term increases in river and sediment discharge determine the dynamics of coastal mudflat and vegetation in the Yangtze Estuary? *Estuarine, Coastal and Shelf Science* **220** 176-184.
[25] Feng, Y and Z Han. 2012 Cellular automata approach to extract shoreline from remote sensing imageries and its application. *J Image Graph* **17** 441-446.